Preparation, Crystal Structures, Conductivities and Electronic Structures of $[et]_3[NiCl_4]\cdot H_2O$ and $[et]_3[AuBr_4]$ [et = bis(ethylenedithio)tetrathiafulvalene]‡

James D. Martin,[a] Enric Canadell,[a] Jonathan C. Fitzmaurice,[b] Alexandra M. Z. Slawin,[b] David J. Williams[b] and J. Derek Woollins*,†,[b]

[a] *Laboratoire de Chimie Theorique (CNRS URA 506), Bat 490, Universite de Paris Sud, 91405 Orsay Cedex, France*

[b] *Department of Chemistry, Imperial College, London SW7 2AY, UK*

Single-crystal studies of $[et]_3[NiCl_4]\cdot H_2O$ and $[et]_3[AuBr_4]$ [et = bis(ethylenedithio)tetrathiafulvalene] have revealed distinctly different packing motifs associated with the different anions. The nickel compound contains a sheet stack structure whilst the gold compound has a herringbone stack of et molecules. The stacking properties are discussed in the context of conductivity and band-theory calculations. The nickel compound exhibits metallic behaviour at room temperature.

The effect of the geometry of the anion upon the structure and properties of charge-transfer salts of bis(ethylenedithio)-tetrathiofulvalene (bedt-ttf or et) is the subject of continuing interest for a number of groups. For example, the crystal structure[1] of β-$[et]_2[AuCl_4]$ consists of et donor layers in the *ab* plane, separated by the layers of $[AuCl_4]^-$ anions along the *c* direction. The plane of each anion is not parallel to the *ab* plane but inclined with a dihedral angle of 35.1°. The donor sheets are more separated in β-$[et]_2[AuCl_4]$ than in β-$[et]_2X$ salts with linear triatomic anions. The crystal structure, semiconducting properties ($\sigma_{rt} \approx 0.05$ S cm^{-1}, $E_a \approx 180$ meV) and temperature-dependent ESR parameters for $[et]_2[Au(CN)_2Cl_2]$ were found to be very similar to those of $[et]_2[QF_6]$ (Q = Sb or As), all of which undergo a broad phase transition near to, or slightly below, room temperature (r.t.).[2] The tetrahedral anionic complexes $[et]_2[FeCl_4]$ and $[et][FeBr_4]$ have been reported.[3] While the former was found to be a semiconductor ($\sigma_{rt} \approx 10^{-2}$ S cm^{-1}, E_a *ca.* 210 meV), the latter was a poor semiconductor ($\sigma_{rt} \approx 10^{-6}$ S cm^{-1}). The chloro complex consists of dimerised stacks of et molecules separated by sheets of tetrahedral $[FeCl_4]^-$ anions, with the shortest intermolecular S···S distances being in the range 3.4–3.52 Å; the α and β forms of $[et]_2[PF_6]$ have nearly identical interstack interactions. This contrasts with the corrugated-sheet network of $[et]_2[ReO_4]$[4] and $[et]_2[BrO_4]$.[5]

The majority of salts studied to date contain tetrahedral or linear anions; here we report studies on the formation of compounds containing square-planar anions. Of particular interest is $[et]_3[NiCl_4]\cdot H_2O$ in which the $[NiCl_4]^{2-}$ anion has a distorted square-planar, rather than the expected tetrahedral geometry. This latter material appears to be isostructural with $[et]_3[CuCl_4]\cdot H_2O$ which has been recently reported.[6]

Experimental

General.—Microanalyses were provided by the Imperial College Microanalytical service. Solvents were dried and distilled by normal methods.

The compound et was prepared by the literature method[7] and recrystallised from chloroform; ttf (Aldrich Chem. Co.) was recrystallised from CH_2Cl_2–cyclohexane. The salts $[NBu_4][AuBr_4]$[8] and $[NBu_4][AuLBr_2]$[9] [L = maleonitriledithiolate (mnt) or ethanedithiolate (edt)] were recrystallised from Pr^iOH, $[AsPh_4]_2[MCl_4]$ (M = Ni[10] or Co[11]) from ethanol–ethyl acetate.

Electrocrystallisations.—A typical experimental set-up involves dissolving the donor compound (5–10 mg) in the chosen solvent (11 cm^3) and placing in the anode compartment; the anionic derivative (10–15 mg) in solvent (12 cm^3) was pipetted into a cathodic cell retaining 1 cm^3 which was added to the donor solution. The solutions were degassed for 30 s, the platinum-wire electrodes placed in the H-cell (solution under argon) and a current of 1 μA cm^{-2} applied using a constant-current source. The H-cells were maintained in a temperature-controlled environment (22 °C) in the dark (to avoid possible photochemical decomposition of the donor).

Electrical Conductivity Studies.—Single-crystal measurements were made using four-probe d.c. techniques with silver–graphite paint as the contact material. Compressed-pellet measurements were used for microcrystalline and powdered samples. The sample mounting was similar to that described by Coleman,[12] using 13 or 25 μm diameter 99.99% pure annealed gold wire. All single-crystal measurements were along the direction of growth; the isotropic (anisotropic) nature of the crystals could not be established due to their size along the other two axes. The use of the term metallic conductivity refers to increasing electrical conductivity (decreasing resistivity) as the temperature is lowered. Forward runs refer to a decrease in the temperature step during conductivity measurements; the obverse is true for reverse runs.

Preparations.—$[et]_3[AuBr_4]$. Electrocrystallisation of a tetrahydrofuran (thf) solution of et (2 mmol dm^{-3}) and $[NBu_4][AuBr_4]$ (3 mmol dm^{-3}) (0.5 μA cm^{-2}) gave black microcrystalline clusters and blocks (Found: C, 21.55; H, 1.40. Calc. for $[et]_3[AuBr_4]$: C, 21.55; H, 1.45%).

A segment cut from one of the blocks was suitable for X-ray diffraction; conductivity measurements were carried out on a

† *Present address:* Department of Chemistry, Loughborough University, Loughborough, LE11 3TU, UK.

‡ More systematically: 4,5-(ethylenedithio)-2-[4′,5-(ethylenedithio)-dithiol-2′-ylidene]-1,3-dithiole.

Supplementary data available: see Instructions for Authors, *J. Chem. Soc., Dalton Trans.*, 1994, Issue 1, pp. xxiii–xxvii.

Non-SI unit employed: eV ≈ 1.60 × 10^{-19} J.

compressed disc of the sample. Hexagonal plates and thin elongated platelets formed at the anode using benzonitrile as the solvent. Owing to the small size of the 'coffin-like' plates, two- (instead of the usual four-) probe conductivity measurements were carried out on the plates. It was not possible to salvage the hexagonal plates intact. Microanalyses (Found: C, 21.30; H, 1.30%) did not provide any conclusive evidence as to the identity of the compound and corresponds closely to the calculated values for $[et]_2[AuBr_2]$, but is also similar to that calculated for $[et]_3[AuBr_4]$, so this cannot be taken as proof of formulation.

A black microcrystalline solid was obtained from electrocrystallisation of ttf and $[NBu_4][AuBr_4]$ in benzonitrile, with approximate stoichiometry $[ttf]_5[AuBr_4]$ (Found: C, 23.85; H, 1.35. Calc. for $[ttf]_5[AuBr_4]$: C, 23.40; H, 1.30%).

α′-$[et]_2[AuBr_2]$. Further investigation into donor/anionic complexes containing square-planar anions was carried out by electrocrystallisation of et with $[NBu_4][Au(mnt)Br_2]$ in thf. After 12 h very thin long plates had formed at the anode. Identical lattice parameters and appropriate elemental analyses revealed the donor salt to be the α′ form of $[et]_2[AuBr_2]$. Variation of the dithiolene to $[Au(edt)Br_2]^-$ and solvent to 1,1,2,2-tetrachloroethane (tce) resulted also in the formation of α′-$[et]_2[AuBr_2]$ (Found: C, 21.35; H, 1.40. Calc. for $[et]_2[AuBr_2]$: C, 21.35; H, 1.45%).

$[et]_3[NiCl_4]\cdot H_2O$. Long black needles of $[et]_3[NiCl_4]\cdot H_2O$ were grown by electrocrystallisation of 3 mmol dm^{-3} et and 5 mmol dm^{-3} $[AsPh_4]_2[Ni(CS_3)_2]$ in tce at a current density of 1 μA cm^{-2}. Black clusters of the compound were also formed at the bottom of the anodic cell. The stoichiometry was determined by X-ray crystallography and confirmed by elemental analyses (Found: C, 26.25; H, 1.90. Calc. for $[et]_3[NiCl_4]\cdot H_2O$: C, 26.25; H, 1.90%).

Reaction of et *and* $[AsPh_4]_2[CoCl_4]$. Long black thin branches were grown by electrocrystallisation of 1.5 mmol dm^{-3} and 3 mmol dm^{-3} $[AsPh_4]_2[CoCl_4]$ in benzonitrile. The solid was not of sufficient quality for X-ray analysis (Found: C, 30.10; H, 1.90; N, 0.65. Calc. for $[et]_4[CoCl_4]\cdot C_7H_5N$: C, 30.65; H, 2.00; N, 0.75%).

Crystallography.—(*a*) $[et]_3[NiCl_4]\cdot H_2O$. *Crystal data.* $C_{30}H_{26}Cl_4NiOS_{24}$, M = 1372.6, triclinic, space group $P\bar{1}$, a = 9.016(2), b = 16.269(3), c = 16.696(2) Å, α = 96.87(1), β = 93.22(1), γ = 90.81(2)°, U = 2427 Å^3, Z = 2, D_c = 1.88 g cm^{-3}. Crystal dimensions 0.10 × 0.10 × 0.36 mm, μ(Cu-Kα) = 125 cm^{-1}, λ = 1.541 78 Å, $F(000)$ = 1388.

Data collection and processing. Nicolet R3m diffractometer, ω-scan method, (2θ ≤ 116°), graphite-monochromated Cu-Kα radiation; 6547 independent measured reflections, 4808 observed [$|F_o| > 3\sigma(|F_o|)$], corrected for Lorentz and polarisation factors; numerical absorption correction (face-indexed crystal), maximum and minimum transmission factors 0.412 and 0.135 respectively.

Structure analysis and refinement. The structure was solved by direct methods and the non-hydrogen atoms refined anisotropically. A ΔF map revealed the presence of a water molecule, the protons of which were not located. The positions of the hydrogen atoms were idealised (C–H 0.96 Å), assigned isotropic thermal parameters U(H) = 1.2U_{eq}(C) and allowed to ride on their parent carbons. Refinement was by block-cascade full-matrix least squares to R = 0.066, R' = 0.066 where $w^{-1} = \sigma^2(F) + 0.00050F^2$. The maximum and minimum residual electron densities in the final ΔF map were 0.98 and −0.59 e Å^{-3} and the mean and maximum shifts/error in the final refinement cycle were 0.006 and 0.026 respectively.

(*b*) $[et]_3[AuBr_4]$. $C_{30}H_{24}AuBr_4S_{24}$, M = 1670.6, monoclinic, space group $P2_1/a$, a = 13.919(4), b = 10.292(4), c = 17.216(4) Å, β = 102.39(2)°, U = 2409 Å^3, Z = 2 (the molecule is disposed about a centre of symmetry), D_c = 2.30 g cm^{-3}. Crystal dimensions 0.13 × 0.18 × 0.23 mm, μ(Cu-Kα) = 197 cm^{-1}, λ = 1.541 78 Å, $F(000)$ = 1614.

Data collection and processing. As above except 2θ ≤ 100°; 2460 independent measured reflections; 2102 observed, maximum and minimum transmission factors 0.198 and 0.058 respectively.

Structure analysis and refinement. The method of structure solution, treatment of non-hydrogen and hydrogen atoms and refinement were as above, giving R = 0.044, R' = 0.048 where $w^{-1} = \sigma^2(F) + 0.001\,00F^2$. The maximum and minimum residual electron densities in the final ΔF map were 1.15 and −0.88 e Å^{-3} and the mean and maximum shifts/error in the final refinement cycle were 0.006 and 0.021 respectively. Computations were performed using the SHELXTL program system.[13]

Additional material available from the Cambridge Crystallographic Data Centre comprises H-atom coordinates, thermal parameters and remaining bond lengths and angles.

Band Structure Calculations.—The tight-binding band-structure calculations[14] were of the extended-Huckel type.[15] A modified Wolfsberg–Helmholz formula was used to calculate the non-diagonal $H_{\mu\nu}$ values.[16] Double-ζ orbitals[17] for C and S were used. The exponents (ζ_μ and ζ_μ'), weighting coefficients (c_μ and c_μ') of the double-ζ orbitals and the $H_{\mu\mu}$ (eV) values used were: 1.831, 1.153, 0.7616, 0.2630 and −21.4 for C 2s: 2.730, 1.257, 0.2595, 0.8025 and −11.4 for C 2p: 2.662, 1.668, 0.5564, 0.4874 and −20.0 for S 3s; and 2.328, 1.333, 0.5208, 0.5439 and −13.3 for S 3p.

Results and Discussion

Crystal Structures and Conductivities.—Long black needles of $[et]_3[NiCl_4]\cdot H_2O$ **1** were obtained serendipitously by electrocrystallisation of $[AsPh_4]_2[Ni(CS_3)_2]$ with et. Although the solvents were dried in duplicate experiments we obtained the same product; the water in the product probably comes from the glassware used. No attempt to use extensively dried glassware was made. The stoichiometry of the compound was determined by X-ray crystallography and satisfactory microanalyses were obtained. The structure and properties of **1** provide a useful comparison with known et–metal halide salts as well as with $[et]_3[AuBr_4]$ **2** described below.

The crystal structure of compound **1** reveals (Fig. 1, Tables 1, 2) a stacked sheet structure (Fig. 2) comprising layers which contain three crystallographically independent et cations. The average charge on the cations is $+\frac{2}{3}$ and there is no crystallographic evidence for any charge localisation amongst the three independent et units. Each et cation has the well established structure[18] with molecular C_i symmetry and no major disorder in the CH_2CH_2 regions. The $[NiCl_4]^{2-}$ anions are situated in planar domains in the so-called 'anion cavity' which is bounded by the CH_2CH_2 groups of the et cations (Fig. 2). The majority of the methylene H · · · Cl distances are in the range 2.70–2.90 Å; however there are two especially short distances [Cl(4) · · · H(7″b) 2.55, Cl(4) · · · C(7) 3.47, Cl(4) · · · H(10c) 2.53 and Cl(4) · · · C(10) 3.46 Å]. A striking feature of the structure is the unusual geometry of the $[NiCl_4]^{2-}$ anion which is distorted square planar rather than the expected tetrahedral; we have commented on this previously.[19] Pairs of $[NiCl_4]^{2-}$ anions are linked by hydrogen bonds through pairs of water molecules to form dimer-like units [Cl(4) · · · O(1) 3.19, Cl(3′) · · · O(1) 3.33 Å, Cl · · · O · · · Cl 127°]. Furthermore, there are short anion–cation Cl · · · S interactions which range between 3.38 and 3.65 Å as well as long-range interactions (3.8–3.9 Å) involving all four chlorine atoms. Clearly, these interactions must play a part in determining the severe distortions from normal tetrahedral geometry observed in the anion. The detailed analysis of the packing of the et cations in the structure is given below together with the results from band-structure calculations.

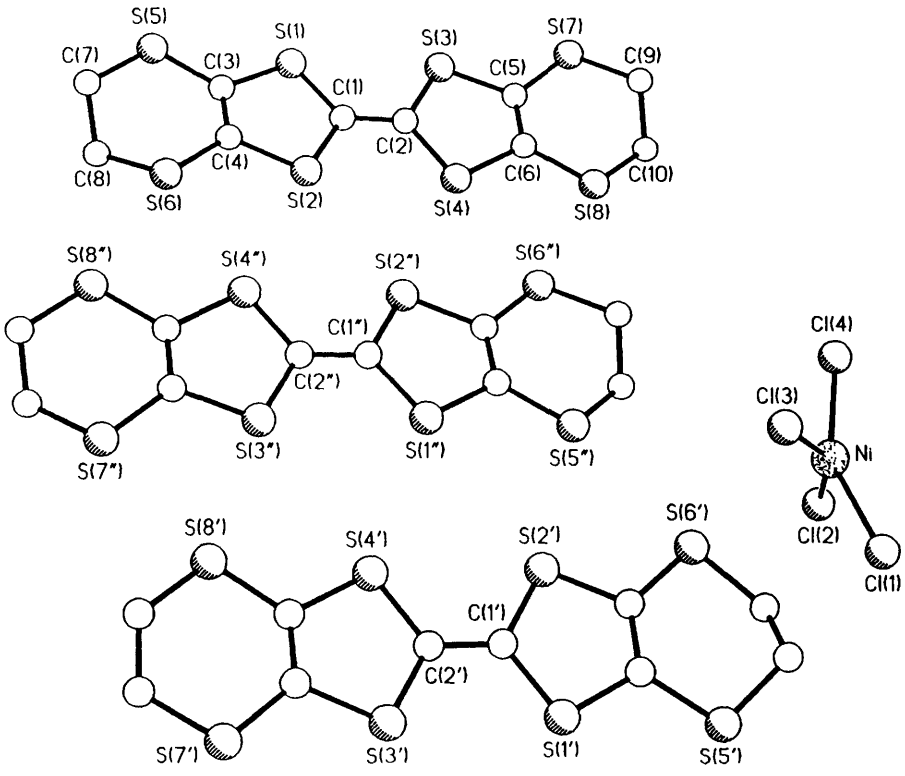

Fig. 1 Crystal structure of compound **1** showing the numbering scheme

Table 1 Atom coordinates ($\times 10^4$) with estimated standard deviations (e.s.d.s) in parentheses for $[et]_3[NiCl_4]\cdot H_2O$

Atom	x	y	z	Atom	x	y	z
Ni	6 316(1)	10 202(1)	7 590(1)	C(4')	1 285(8)	7 631(4)	8 607(4)
Cl(1)	5 492(3)	10 638(1)	8 825(1)	C(5')	−1 950(8)	4 023(4)	8 458(4)
Cl(2)	8 683(3)	9 998(1)	8 074(1)	C(6')	−1 388(8)	3 983(4)	7 728(4)
Cl(3)	4 066(3)	9 694(1)	7 121(1)	S(5')	884(3)	8 479(1)	10 133(1)
Cl(4)	7 047(4)	10 489(2)	6 367(1)	S(6')	2 191(2)	8 411(1)	8 176(1)
C(1)	4 285(8)	5 254(4)	8 372(4)	S(7')	−3 021(3)	3 287(1)	8 850(1)
C(2)	3 630(8)	4 492(4)	8 176(4)	S(8')	−1 557(3)	3 176(1)	6 947(1)
S(1)	4 073(2)	5 851(1)	9 295(1)	C(7')	1 514(12)	9 310(5)	9 632(5)
S(2)	5 341(2)	5 725(1)	7 709(1)	C(8')	2 610(12)	9 128(5)	9 056(6)
S(3)	2 648(2)	3 998(1)	8 858(1)	C(9')	−2 847(14)	2 413(5)	8 111(5)
S(4)	3 733(2)	3 933(1)	7 233(1)	C(10')	−2 803(14)	2 503(6)	7 312(6)
C(3)	5 184(8)	6 690(4)	9 098(4)	C(1")	2 349(8)	4 918(4)	4 991(4)
C(4)	5 773(8)	6 618(4)	8 371(4)	C(2")	1 686(8)	4 154(4)	4 802(4)
C(5)	2 372(8)	3 069(4)	8 227(4)	S(1")	2 218(2)	5 518(1)	5 916(1)
C(6)	2 900(8)	3 026(4)	7 486(4)	S(2")	3 415(2)	5 360(1)	4 312(1)
S(5)	5 275(3)	7 519(1)	9 862(1)	S(3")	698(2)	3 670(1)	5 482(1)
S(6)	6 946(2)	7 334(1)	8 004(1)	S(4")	1 803(2)	3 582(1)	3 862(1)
S(7)	1 450(3)	2 297(1)	8 656(1)	C(3")	3 270(8)	6 352(4)	5 678(4)
S(8)	2 816(3)	2 190(1)	6 719(1)	C(4")	3 860(8)	6 272(4)	4 948(4)
C(7)	6 517(9)	8 250(5)	9 484(5)	C(5")	381(8)	2 731(4)	4 854(4)
C(8)	6 391(10)	8 267(5)	8 579(5)	C(6")	923(8)	2 688(4)	4 109(4)
C(9)	1 854(9)	1 393(5)	7 984(5)	S(5")	3 457(3)	7 190(1)	6 439(1)
C(10)	1 571(9)	1 475(4)	7 103(4)	S(6")	5 003(3)	6 968(1)	4 546(1)
C(1')	65(8)	6 194(4)	8 649(4)	S(7")	−567(2)	1 963(1)	5 270(1)
C(2')	−533(8)	5 408(4)	8 453(4)	S(8")	869(2)	1 854(1)	3 346(1)
S(1')	−77(2)	6 753(1)	9 586(1)	C(7")	4 890(9)	7 796(5)	6 079(5)
S(2')	1 023(2)	6 701(1)	7 974(1)	C(8")	4 732(10)	7 909(5)	5 204(5)
S(3')	−1 540(2)	4 925(1)	9 124(1)	C(9")	−166(12)	1 070(5)	4 605(5)
S(4')	−365(2)	4 845(1)	7 518(1)	C(10")	−303(11)	1 117(5)	3 745(5)
C(3')	770(8)	7 658(4)	9 350(4)	O	6 782(7)	9 511(4)	4 589(4)

Conductivity measurements (four-probe along the needle axis using silver paste to form the contacts*) on single crystals of compound **1** indicate metallic behaviour with a room-temperature conductivity of 20 S cm^{-1}. Initial results on crystal **a** showed metallic behaviour, with the conductivity at 120 K twice the room-temperature value (Fig. 3). Unfortunately this crystal was subjected to a current surge and therefore lost. A second crystal **b** showed slightly different behaviour with a conductivity maximum at 150 K, whereupon a slight decrease in conductivity occurs to a plateau between 140 and 90 K (Fig. 4)

* The colloidal silver paste employed may react with sulfur and the halide of the anion, as pointed out by a referee. We have no evidence to support or refute this suggestion.

Table 2 Bond lengths (Å) and angles (°) for $[et]_3[NiCl_4]\cdot H_2O$ with e.s.d.s in parentheses

Ni–Cl(1)	2.266(2)	Ni–Cl(2)	2.244(3)	C(3′)–C(4′)	1.345(10)	C(3′)–S(5′)	1.750(7)
Ni–Cl(3)	2.244(2)	Ni–Cl(4)	2.279(3)	C(4′)–S(6′)	1.746(8)	C(5′)–C(6′)	1.341(10)
C(1)–C(2)	1.361(10)	C(1)–S(1)	1.742(7)	C(5′)–S(7′)	1.737(8)	C(6′)–S(8′)	1.735(7)
C(1)–S(2)	1.738(8)	C(2)–S(3)	1.742(8)	S(5′)–C(7′)	1.775(10)	S(6′)–C(8′)	1.782(9)
C(2)–S(4)	1.729(7)	S(1)–C(3)	1.755(8)	S(7′)–C(9′)	1.782(9)	S(8′)–C(10′)	1.742(12)
S(2)–C(4)	1.744(7)	S(3)–C(5)	1.742(7)	C(7′)–C(8′)	1.427(15)	C(9′)–C(10′)	1.361(14)
S(4)–C(6)	1.752(7)	C(3)–C(4)	1.344(11)	C(1″)–C(2″)	1.365(9)	C(1″)–S(1″)	1.736(7)
C(3)–S(5)	1.740(7)	C(4)–S(6)	1.749(8)	C(1″)–S(2″)	1.739(8)	C(2″)–S(3″)	1.736(8)
C(5)–C(6)	1.345(10)	C(5)–S(7)	1.743(8)	C(2″)–S(4″)	1.735(7)	S(1″)–C(3″)	1.742(7)
C(6)–S(8)	1.751(7)	S(5)–C(7)	1.813(8)	S(2″)–C(4″)	1.746(7)	S(3″)–C(5″)	1.757(7)
S(6)–C(8)	1.789(8)	S(7)–C(9)	1.795(8)	S(4″)–C(6″)	1.750(7)	C(3″)–C(4″)	1.350(10)
S(8)–C(10)	1.802(8)	C(7)–C(8)	1.512(11)	C(3″)–S(5″)	1.748(7)	C(4″)–S(6″)	1.740(8)
C(9)–C(10)	1.501(11)	C(1′)–C(2′)	1.376(9)	C(5″)–C(6″)	1.358(10)	C(5″)–S(7″)	1.736(8)
C(1′)–S(1′)	1.726(7)	C(1′)–S(2′)	1.733(8)	C(6″)–S(8″)	1.744(7)	S(5″)–C(7″)	1.787(9)
C(2′)–S(3′)	1.732(8)	C(2′)–S(4′)	1.729(7)	S(6″)–C(8″)	1.803(8)	S(7″)–C(9″)	1.775(9)
S(1′)–C(3′)	1.745(7)	S(2′)–C(4′)	1.744(7)	S(8″)–C(10″)	1.799(9)	C(7″)–C(8″)	1.493(12)
S(3′)–C(5′)	1.755(7)	S(4′)–C(6′)	1.748(7)	C(9″)–C(10″)	1.446(12)		
Cl(1)–Ni–Cl(2)	93.9(1)	Cl(1)–Ni–Cl(3)	92.4(1)	C(4′)–C(3′)–S(5′)	128.4(6)	S(2′)–C(4′)–C(3′)	116.8(6)
Cl(2)–Ni–Cl(3)	149.9(1)	Cl(1)–Ni–Cl(4)	150.0(1)	S(2′)–C(4′)–S(6′)	114.5(4)	C(3′)–C(4′)–S(6′)	128.7(5)
Cl(2)–Ni–Cl(4)	93.9(1)	Cl(3)–Ni–Cl(4)	95.2(1)	S(3′)–C(5′)–C(6′)	116.7(5)	S(3′)–C(5′)–S(7′)	114.6(4)
C(2)–C(1)–S(1)	122.6(6)	C(2)–C(1)–S(2)	122.8(6)	C(6′)–C(5′)–S(7′)	128.6(5)	S(4′)–C(6′)–C(5′)	117.1(5)
S(1)–C(1)–S(2)	114.6(4)	C(1)–C(2)–S(3)	122.7(6)	S(4′)–C(6′)–S(8′)	114.9(4)	C(5′)–C(6′)–S(8′)	128.0(6)
C(1)–C(2)–S(4)	122.4(6)	S(3)–C(2)–S(4)	114.9(4)	C(3′)–S(5′)–C(7′)	102.0(4)	C(4′)–S(6′)–C(8′)	100.0(4)
C(1)–S(1)–C(3)	95.9(4)	C(1)–S(2)–C(4)	95.5(4)	C(5′)–S(7′)–C(9′)	101.0(4)	C(6′)–S(8′)–C(10′)	102.2(4)
C(2)–S(3)–C(5)	95.3(3)	C(2)–S(4)–C(6)	95.7(3)	S(5′)–C(7′)–C(8′)	117.0(7)	S(6′)–C(8′)–C(7′)	120.1(7)
S(1)–C(3)–C(4)	116.0(5)	S(1)–C(3)–S(5)	114.3(4)	S(7′)–C(9′)–C(10′)	121.1(7)	S(8′)–C(10′)–C(9′)	122.8(8)
C(4)–C(3)–S(5)	129.6(6)	S(2)–C(4)–C(3)	117.8(6)	C(2″)–C(1″)–S(1″)	123.5(6)	C(2″)–C(1″)–S(2″)	121.8(5)
S(2)–C(4)–S(6)	115.2(4)	C(3)–C(4)–S(6)	126.9(6)	S(1″)–C(1″)–S(2″)	114.8(4)	C(1″)–C(2″)–S(3″)	123.0(5)
S(3)–C(5)–C(6)	117.5(5)	S(3)–C(5)–S(7)	114.5(4)	C(1″)–C(2″)–S(4″)	122.2(6)	S(3″)–C(2″)–S(4″)	114.7(4)
C(6)–C(5)–S(7)	128.0(5)	S(4)–C(6)–C(5)	116.3(5)	C(1″)–S(1″)–C(3″)	95.7(3)	C(1″)–S(2″)–C(4″)	95.7(3)
S(4)–C(6)–S(8)	115.1(4)	C(5)–C(6)–S(8)	128.6(6)	C(2″)–S(3″)–C(5″)	96.0(3)	C(2″)–S(4″)–C(6″)	96.0(3)
C(3)–S(5)–C(7)	103.0(4)	C(4)–S(6)–C(8)	99.9(4)	S(1″)–C(3″)–C(4″)	117.1(5)	S(1″)–C(3″)–S(5″)	114.9(4)
C(5)–S(7)–C(9)	101.4(4)	C(6)–S(8)–C(10)	102.3(3)	C(4″)–C(3″)–S(5″)	128.0(6)	S(2″)–C(4″)–C(3″)	116.7(6)
S(5)–C(7)–C(8)	115.2(5)	S(6)–C(8)–C(7)	114.3(6)	S(2″)–C(4″)–S(6″)	114.9(4)	C(3″)–C(4″)–S(6″)	128.4(5)
S(7)–C(9)–C(10)	114.8(5)	S(8)–C(10)–C(9)	114.3(5)	S(3″)–C(5″)–C(6″)	116.2(5)	S(3″)–C(5″)–S(7″)	115.9(4)
C(2′)–C(1′)–S(1′)	122.6(6)	C(2′)–C(1′)–S(2′)	122.7(5)	C(6″)–C(5″)–S(7″)	127.9(5)	S(4″)–C(6″)–C(5″)	116.8(5)
S(1′)–C(1′)–S(2′)	114.6(4)	C(1′)–C(2′)–S(3′)	122.0(5)	S(4″)–C(6″)–S(8″)	114.4(4)	C(5″)–C(6″)–S(8″)	128.8(6)
C(1′)–C(2′)–S(4′)	122.4(6)	S(3′)–C(2′)–S(4′)	115.5(4)	C(3″)–S(5″)–C(7″)	101.7(4)	C(4″)–S(6″)–C(8″)	101.5(4)
C(1′)–S(1′)–C(3′)	96.0(3)	C(1′)–S(2′)–C(4′)	95.8(3)	C(5″)–S(7″)–C(9″)	101.4(4)	C(6″)–S(8″)–C(10″)	102.2(4)
C(2′)–S(3′)–C(5′)	95.3(3)	C(2′)–S(4′)–C(6′)	95.3(3)	S(5″)–C(7″)–C(8″)	115.8(6)	S(6″)–C(8″)–C(7″)	113.0(6)
S(1′)–C(3′)–C(4′)	116.6(5)	S(1′)–C(3′)–S(5′)	115.0(4)	S(7″)–C(9″)–C(10″)	118.4(6)	S(8″)–C(10″)–C(9″)	117.7(6)

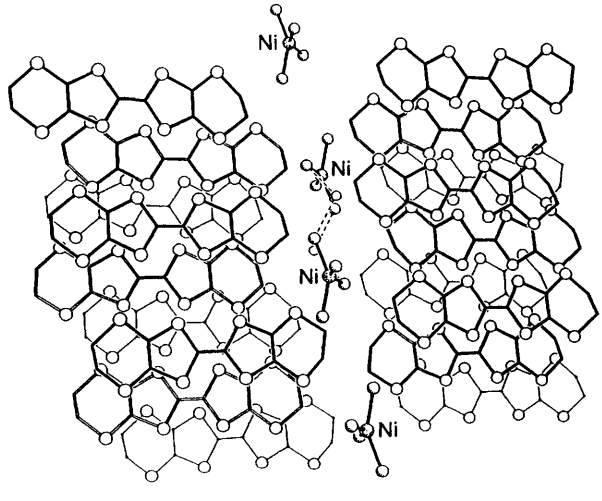

Fig. 2 Crystal structure of compound **1** showing the stacking of the et cations and the $[NiCl_4]^{2-}$ anions

and then a further decrease to semimetallic behaviour at the lowest temperature measured (20 K, $\sigma \approx 12$ S cm^{-1}). The $\ln(\sigma/\sigma_{rt})$ *versus* T curve can be approximated by the phenomenological model proposed by Epstein *et al.*[20] but only a poor fit could be obtained here.

Upon cooling crystal **b** from room temperature on a repeat run, it was found to have undergone an 'irreversible' structural phase change, as evidenced by the conductivity plot (Fig. 5). A plot of $\ln(\sigma/\sigma_{rt})$ *versus* T indicates semiconducting behaviour with a high room-temperature conductivity of 20 S cm^{-1}, decreasing to $\approx$6 S cm^{-1} at 55 K. The T^{-1} dependence is non-linear, implying a two-dimensionality to the compound. An estimation of the activation energy for the temperature range 290–135 K is $E_a \approx 15$ meV. The conductivity properties of compound **1** are quite similar to those of the different phases of [et]Cl reported by Rosseinsky *et al.*,[21,22] but microanalyses coupled with vibrational spectroscopic studies support the formulation given here for the bulk material; furthermore, unit-cell parameters were checked for a number of crystals and found to be reproducible.

It is of interest to compare $[et]_3[NiCl_4]\cdot H_2O$ and crystalline salts obtained from electrocrystallisation of et and $[AsPh_4]_2[NiCl_4]$. Electrocrystallisation of et and $[AsPh_4]_2[NiCl_4]$ in benzonitrile yielded whisker shapes of $[et]_x[NiCl_4]$ at the anode. The room-temperature conductivity was 5 S cm^{-1} with only a slight increase to 250 K [$d\sigma/dT \approx 1.3 \times 10^{-3}$ S cm^{-1} K^{-1}) (Fig. 6); a further decrease in temperature resulted in a sharp transition at 140 K to a semiconducting state with $\sigma \approx 10^{-1}$ S cm^{-1} at 50 K. While crystals were of insufficient quality for X-ray analysis, conductivity measurements show the compound to be of poor metallic nature with a transition to a semiconducting state at approximately 140 K. Since $[et]_3[NiCl_4]\cdot H_2O$ was obtained by chance, possibly due to chlorine abstraction from tce, the formation of the $[NiCl_4]^{2-}$

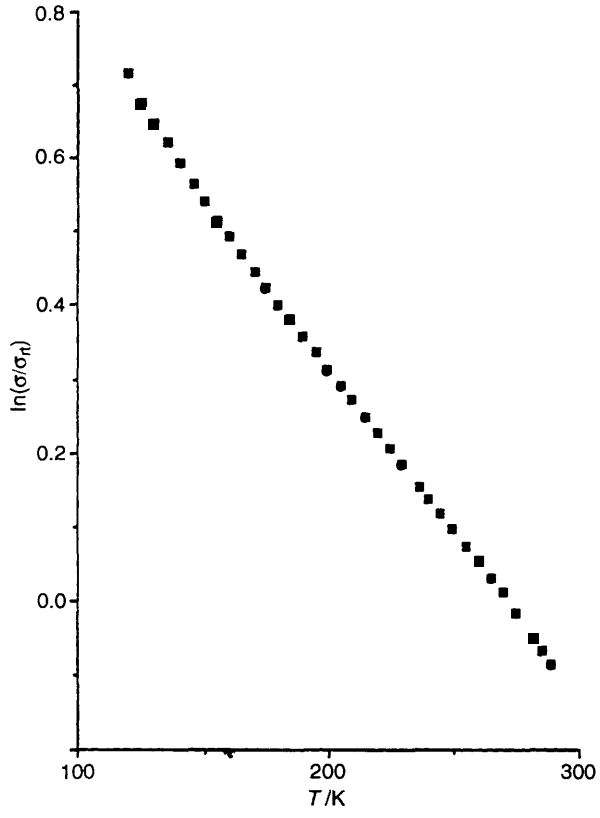

Fig. 3 Plot of $\ln(\sigma/\sigma_{rt})$ *versus* temperature for $[et]_3[NiCl_4]\cdot H_2O$ **1** (single crystal **a**)

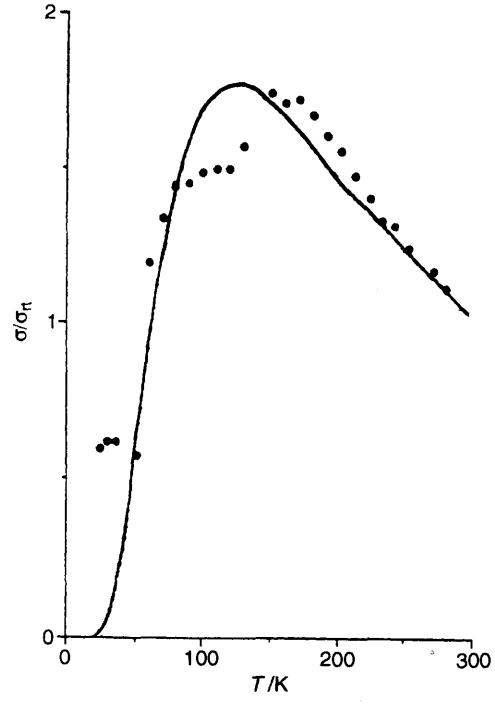

Fig. 4 Plot of σ/σ_{RT} *versus* temperature for $[et]_3[NiCl_4]\cdot H_2O$ **1** (single crystal **b**) and 'best fit' to the expression $\exp(-\Delta H/K_B T)\cdot T^{-\alpha}$ where $\Delta H = 19.3$ meV and $\alpha = 1.82$

ion and its geometry may be determined by the interaction of the donor molecules and short donor H · · · Cl contacts, which are known to exist. Hence, the unusual geometry of $[NiCl_4]^{2-}$ in compound **1** allows important interactions to occur, which is reflected in the electrical properties; metallic behaviour is

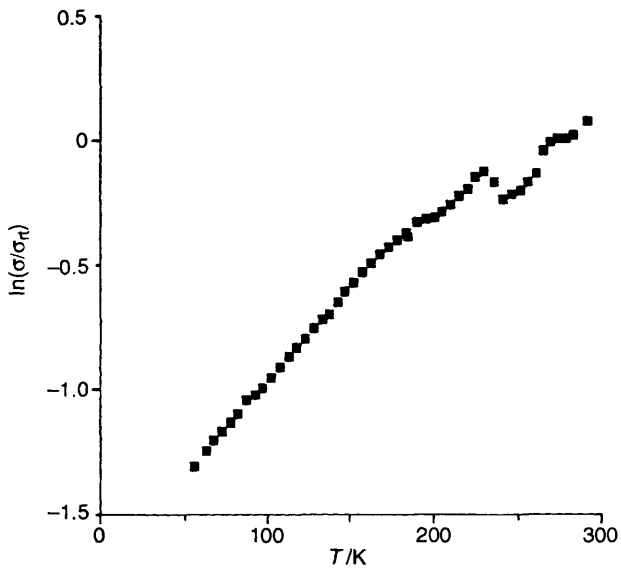

Fig. 5 Plot of $\ln(\sigma/\sigma_{rt})$ *versus* temperature for $[et]_3[NiCl_4]\cdot H_2O$ **1** (single crystal **b**) after phase change

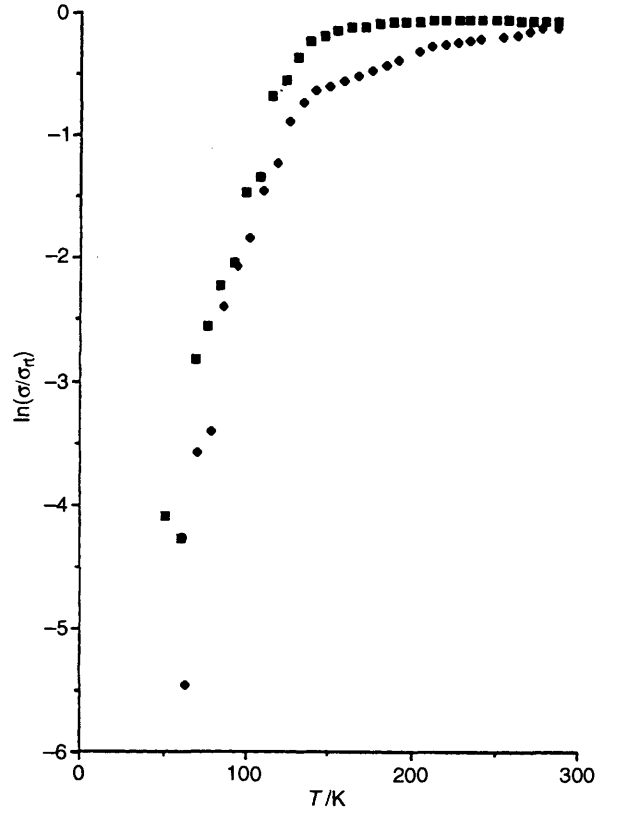

Fig. 6 Plot of $\ln(\sigma/\sigma_{rt})$ *versus* temperature for an $[et]_3[NiCl_4]\cdot H_2O$ whisker obtained from benzonitrile: (■), forward run; (◆), reverse run

observed to reasonably low temperatures (120 K) with moderate conductivity at room temperature ($\sigma_{rt} = 20$ S cm^{-1}).

Electrocrystallisation of a thf solution of et and $[NBu_4][AuBr_4]$ gave black microcrystalline clusters and blocks of $[et]_3[AuBr_4]$ **2**. The crystal structure of compound **2** (Fig. 7, Tables 3 and 4) is very different from that of **1**. The 3:1 stoichiometry is retained with the asymmetric unit containing 1.5 et units and 0.5 $[AuBr_4]^-$ anions. One of the et molecules is positioned about a crystallographic centre of symmetry whilst the $[AuBr_4]^-$ lies on another. As in **1** the et molecules have

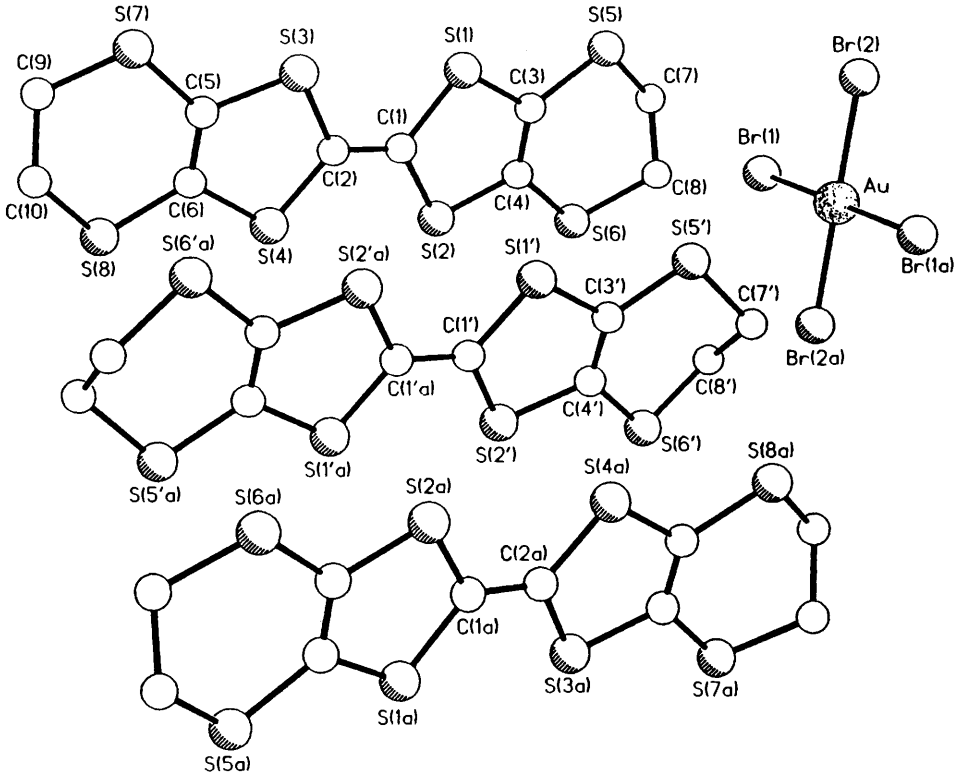

Fig. 7 Crystal structure of compound **2** showing the numbering scheme

Table 3 Atomic coordinates ($\times 10^4$) for $[et]_3[AuBr_4]$ with e.s.d.s in parentheses

Atom	*x*	*y*	*z*
Au	5000	5000	0
Br(1)	3839(1)	3297(1)	249(1)
Br(2)	3816(1)	6692(1)	207(1)
C(1)	6933(8)	4851(9)	5227(6)
S(1)	6066(2)	6039(3)	4823(1)
S(2)	7122(2)	3681(3)	4537(1)
C(3)	5781(8)	5365(10)	3870(5)
C(4)	6268(7)	4315(11)	3743(5)
S(5)	4876(2)	6252(3)	3207(2)
S(6)	6152(2)	3450(3)	2853(2)
C(7)	4665(8)	5212(11)	2341(6)
C(8)	5544(8)	4654(11)	2152(6)
C(2)	7397(7)	4862(9)	5985(6)
S(3)	7189(2)	6082(3)	6632(1)
S(4)	8252(2)	3700(3)	6418(1)
C(5)	7938(7)	5422(10)	7484(6)
C(6)	8408(7)	4330(11)	7382(5)
S(7)	7925(2)	6263(3)	8353(1)
S(8)	9190(2)	3390(3)	8121(1)
C(9)	8406(9)	5073(10)	9075(6)
C(10)	9332(9)	4473(10)	8965(6)
C(1')	9769(8)	4988(10)	4607(6)
S(1')	8979(2)	6228(3)	4191(1)
S(2')	9936(2)	3774(3)	3957(2)
C(3')	8767(7)	5612(12)	3222(5)
C(4')	9200(8)	4491(10)	3117(6)
S(5')	7979(2)	6567(3)	2526(2)
S(6')	9122(2)	3607(3)	2238(2)
C(7')	8125(9)	5828(12)	1606(6)
C(8')	8069(8)	4327(11)	1614(6)

molecular C_i symmetry, with no noticeable disorder in the CH_2CH_2 units of the independent molecules. There is some evidence for charge localisation with the C(1)–C(2) and C(1')–C(1'a) distances differing [1.326(13) and 1.368(19) Å respectively]. Both the differences in the bond lengths and the

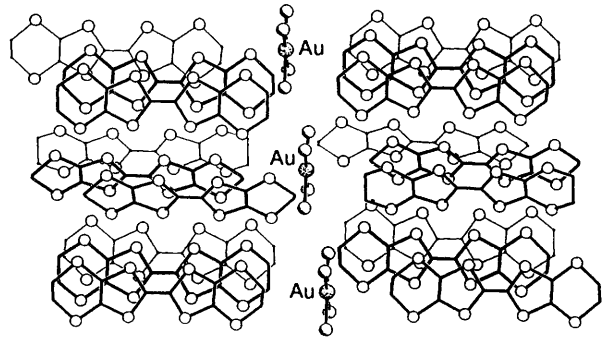

Fig. 8 Crystal structure of compound **2** showing the stacking of the et cations and the $[AuBr_4]^-$ anions

band-structure calculations (below) indicate that the two different et cations have formal charges of 0 and +1. In common with **1** the anions reside in an essentially planar domain sandwiched between the CH_2CH_2 groups. However, on going from $[NiCl_4]^{2-}$ to $[AuBr_4]^-$ the stacking motif of the et molecules is dramatically modified (Fig. 8). Interanion and anion–cation distances in **2** are all long. The shortest interanion Br···Br distance is 3.97 Å (*cf.* 3.50 Å for the *cis* intramolecular Br···Br distance). The shortest anion–cation distance is 2.89 Å (Br···H) with a corresponding Br···C distance of 3.84 Å.

Compressed-disc conductivity measurements on $[et]_3[AuBr_4]$ **2** reveal it to be a semiconductor ($\sigma_{rt} \approx 0.25$ S cm^{-1}) (Fig. 9) with low activation energy ($E_a \approx 25$ meV) which undergoes a transition at 125 K to an insulating phase at lower temperatures.

Electrocrystallisation of et and $[NBu_4][AuBr_4]$ in benzonitrile gave small thin plates; owing to the size, two-probe conductivity measurements were carried out and the results suggest a different stoichiometry or new phase. The plates exhibited semiconducting properties ($\sigma_{rt} \approx 2.2 \times 10^{-3}$ S cm^{-1}) with large activation energies ($E_a = 205$, $E_g = 410$ meV). The compound behaves as an insulator at temperatures less

Table 4 Bond lengths (Å) and angles (°) for $[et]_3[AuBr_4]$ with e.s.d.s in parentheses

Au–Br(1)	2.483(1)	Au–Br(2)	2.476(1)	S(4)–C(6)	1.752(10)	C(5)–C(6)	1.331(15)
Au–Br(1a)	2.483(1)	Au–Br(2a)	2.476(1)	C(5)–S(7)	1.731(10)	C(6)–S(8)	1.773(10)
C(1)–S(1)	1.754(10)	C(1)–S(2)	1.750(11)	S(7)–C(9)	1.771(11)	S(8)–C(10)	1.807(11)
C(1)–C(2)	1.326(13)	S(1)–C(3)	1.746(10)	C(9)–C(10)	1.478(17)	C(1′)–S(1′)	1.736(11)
S(2)–C(4)	1.735(9)	C(3)–C(4)	1.319(15)	C(1′)–S(2′)	1.727(11)	C(1′)–C(1′a)	1.368(19)
C(3)–S(5)	1.762(10)	C(4)–S(6)	1.749(10)	S(1′)–C(3′)	1.749(10)	S(2′)–C(4′)	1.747(10)
S(5)–C(7)	1.807(11)	S(6)–C(8)	1.809(11)	C(3′)–C(4′)	1.332(16)	C(3′)–S(5′)	1.745(10)
C(7)–C(8)	1.450(17)	C(2)–S(3)	1.743(10)	C(4′)–S(6′)	1.749(10)	S(5′)–C(7′)	1.808(12)
C(2)–S(4)	1.738(10)	S(3)–C(5)	1.745(9)	S(6′)–C(8′)	1.782(10)	C(7′)–C(8′)	1.547(17)
Br(1)–Au–Br(2)	89.6(1)	Br(1)–Au–Br(1a)	180.0(1)	S(3)–C(5)–C(6)	116.1(7)	S(3)–C(5)–S(7)	114.6(6)
Br(2)–Au–Br(1a)	90.4(1)	Br(1)–Au–Br(2a)	90.4(1)	C(6)–C(5)–S(7)	129.2(7)	S(4)–C(6)–C(5)	118.2(7)
Br(2)–Au–Br(2a)	180.0(1)	Br(1a)–Au–Br(2a)	89.6(1)	S(4)–C(6)–S(8)	114.2(6)	C(5)–C(6)–S(8)	127.6(7)
S(1)–C(1)–S(2)	113.6(5)	S(1)–C(1)–C(2)	122.2(8)	C(5)–S(7)–C(9)	100.9(5)	C(6)–S(8)–C(10)	100.6(5)
S(2)–C(1)–C(2)	124.1(8)	C(1)–S(1)–C(3)	95.4(5)	S(7)–C(9)–C(10)	114.0(8)	S(8)–C(10)–C(9)	114.4(7)
C(1)–S(2)–C(4)	95.7(5)	S(1)–C(3)–C(4)	117.4(7)	S(1′)–C(1′)–S(2′)	115.2(6)	S(1′)–C(1′)–C(1′a)	121.1(12)
S(1)–C(3)–S(5)	112.9(6)	C(4)–C(3)–S(5)	129.6(7)	S(2′)–C(1′)–C(1′a)	123.7(11)	C(1′)–S(1′)–C(3′)	95.1(5)
S(2)–C(4)–C(3)	117.8(7)	S(2)–C(4)–S(6)	114.7(6)	C(1′)–S(2′)–C(4′)	95.4(5)	S(1′)–C(3′)–C(4′)	117.1(7)
C(3)–C(4)–S(6)	127.5(7)	C(3)–S(5)–C(7)	101.2(5)	S(1′)–C(3′)–S(5′)	113.8(6)	C(4′)–C(3′)–S(5′)	129.1(7)
C(4)–S(6)–C(8)	100.2(5)	S(5)–C(7)–C(8)	115.1(7)	S(2′)–C(4′)–C(3′)	117.0(7)	S(2′)–C(4′)–S(6′)	114.4(6)
S(6)–C(8)–C(7)	114.7(8)	C(1)–C(2)–S(3)	121.5(8)	C(3′)–C(4′)–S(6′)	128.6(7)	C(3′)–S(5′)–C(7′)	101.1(5)
C(1)–C(2)–S(4)	124.1(8)	S(3)–C(2)–S(4)	114.4(5)	C(4′)–S(6′)–C(8′)	101.2(5)	S(5′)–C(7′)–C(8′)	113.3(8)
C(2)–S(3)–C(5)	96.1(5)	C(2)–S(4)–C(6)	95.0(5)	S(6′)–C(8′)–C(7′)	112.6(7)		

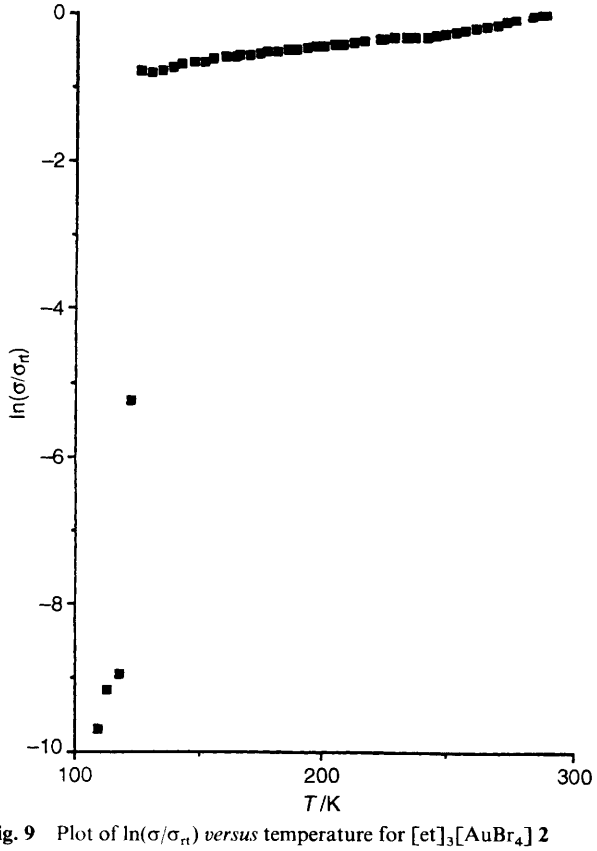

Fig. 9 Plot of $\ln(\sigma/\sigma_{rt})$ *versus* temperature for $[et]_3[AuBr_4]$ **2**

than 150 K. Only X-ray diffraction studies can reveal the stoichiometry (and phase) of the compound.

Electronic Structures.—A view of the *ac* slab of $[et]_3[NiCl_4]\cdot H_2O$ **1** is shown in Fig. 10. The et molecules stack so that each is surrounded by six neighbouring molecules, two above, two below and two approximately within the et molecular plane. A total of eleven intermolecular contacts [see Fig. 10(*b*)] are observed between the three crystallographically distinct molecules in the structure of **1**. The shortest intermolecular S···S distances, considerably less than the sum of their van der Waals radii, are found for the in-plane type contacts, *A* (see

Table 5 Intermolecular S···S distances less than 3.8 Å and overlap integrals ($\times 10^{-3}$) associated with the et···et interactions in compound **1**

Interaction	S···S/Å	Overlap (10^{-3})
A_1	3.335, 3.401, 3.433, 3.452, 3.799	6.2
A_2	3.397, 3.427, 3.566, 3.617	5.7
A_3	3.359, 3.414, 3.441, 3.540	5.7
B_1	3.629, 3.716, 3.771	10.6
B_2	3.793, 3.771	10.5
B_3	3.722 (2×)	10.1
B_4	3.729 (2×)	7.8
C_1	3.801	2.6
C_2	(3.833)	3.0
C_3	(3.850)	3.0
C_4	3.775 (2×)	2.2

distances in Table 5). The intermolecular contacts of type *B* exhibit contacts as short as 3.629 Å. However, in the stacks along the *a* axis only contact C_4 exhibits an S···S contact shorter than 3.8 Å. The in-plane *a* contacts, *A*, give rise to intermolecular π-type interactions resulting in small overlap integrals (Table 5) in spite of the short contacts. The *B* and *C* type contacts give rise to three different types of slipped stacks: *B*, C_1–C_2 and C_3–C_4 are associated with the sequences of interactions B_3–B_1–B_2–B_4–B_2–B_1–B_3 . . ., C_1–C_2–C_1 . . . and C_3–C_4–C_3 . . ., respectively. All of them form σ-type interactions between highest-occupied molecular orbitals (HOMOs) of adjacent molecules. Consequently, in spite of the longer distances, the overlaps calculated for contacts *B* are significantly greater than those of *A*. The overlaps calculated for contacts *C* reflect the greatly increased intermolecular distances.

Since the repeating unit in the *ac* slab of compound **1** contains six et molecules, the calculated electronic band structure (Fig. 11) contains six bands derived from the HOMOs of the et molecules. Although these slabs contain three crystallographically distinct et molecules, their respective HOMOs are very similar: all within an energy range of 0.07 eV. Thus, a strong mixing of the HOMOs of the three crystallographically independent molecules is observed in the HOMO bands of this slab. Nevertheless, the weak overlap calculated for the stacks along the *a* axis is consistent with the lesser dispersion observed for the HOMO bands along Γ to *X*.

The formal oxidation of the et molecules ($+\frac{2}{3}$) required by the stoichiometry provides eight electrons to fill the six bands described above. The resulting Fermi level cuts the fourth and

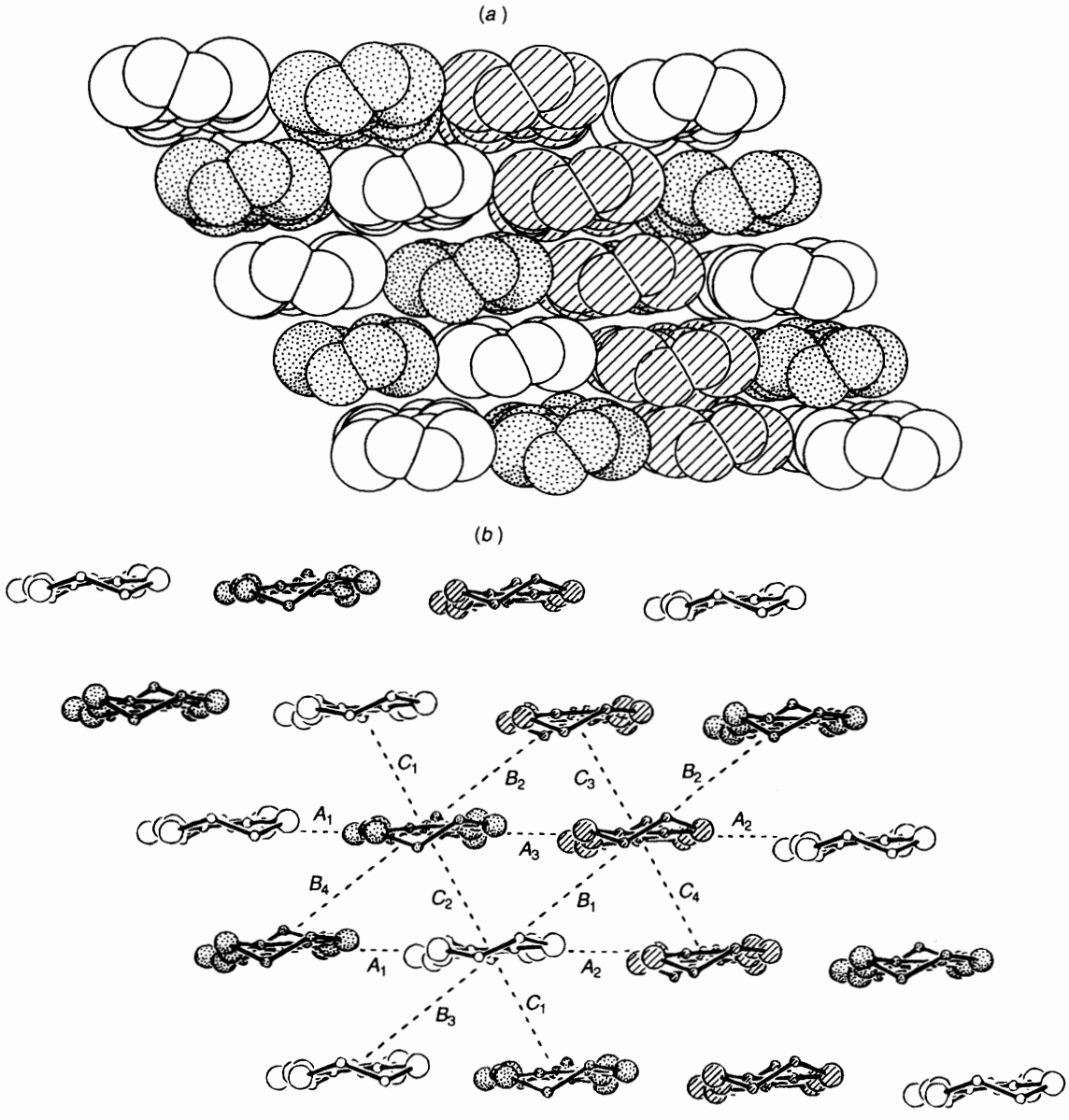

Fig. 10 Space filling (protons omitted for clarity) (*a*) and conventional ball-and-stick (*b*) views of the *ac* slab in compound **1**, looking down the et molecular plane, indicating the molecular contacts. The crystallographically independent molecules are signified using different shadings

fifth bands (from the bottom). Since both of these bands exhibit reasonable dispersion for et salts (0.2–0.25 eV), **1** is expected to exhibit metallic conductivity, in agreement with the conductivity measurements. The Fermi level cutting bands four and five gives the Fermi surface with hole pockets centred at Γ and electron pockets centred at *Z*, respectively (Fig. 12). With the elongated hole pockets lying along the vector a^* and the electron pocket elongated along the vector c^*–a^*, **1** is expected to be a two-dimensional metal, though with somewhat better conductivity along the $a + c$ direction.

In the light of the calculated band structure and Fermi surface, it is interesting to consider the origin of the observed metal to semiconductor transition observed between 150 and 90 K. While the anomalous resistivity behaviour observed in this range may be an artifact of the physical measurement, we note that the Fermi surface will be exceedingly sensitive to minor structural changes due to flat regions around the Fermi level (see in particular Γ to *X* of Fig. 12). Since no nesting vectors exist which simultaneously nest the entire hole and the electron surfaces,[23] the transition is not the result of a Peierls distortion. The change in the conductivity regime near 150 K can originate from (*a*) an electron localisation or (*b*) the semimetallic overlap

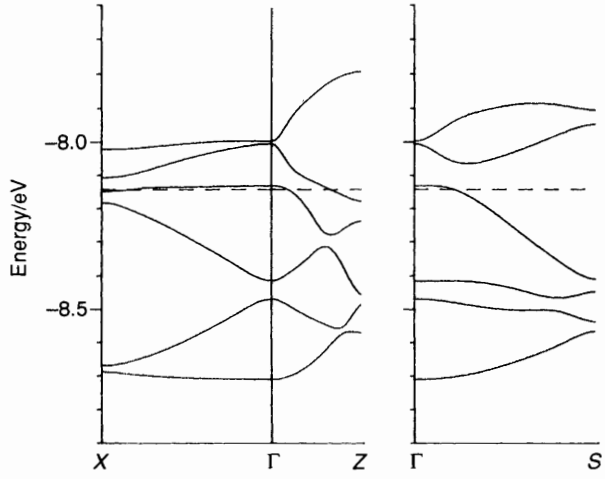

Fig. 11 Band structure of the et slab in compound **1**. The dashed line indicates the Fermi level and Γ, *X*, *Z* and *S* refer to the wave vectors (0, 0), $(\frac{a^*}{2}, 0)$, $(0, \frac{c^*}{2})$ and $(-\frac{a^*}{2}, \frac{c^*}{2})$ respectively

of the fourth and fifth bands in Fig. 11. Owing to the small overlap of these partially filled bands (< 0.05 eV), minor structural modifications upon cooling may suppress this semimetallic overlap leading to a band gap and hence semiconducting behaviour. Magnetic susceptibility measurements are needed in order to distinguish between the possibilities. However, it should be noted that the analogous $[et]_3[CuCl_4]\cdot H_2O$ salt retains its metallic behaviour down to 0.2 K. Thus we are tempted to suggest that an electron localisation induced by some disorder in the included water molecules is the more likely origin for the metal to semiconductor transition in compound **1**. Subtle variations of the solvent in the crystal lattice may also be responsible for the sample dependence of the conductivity and the permanence of the semiconductor behaviour after cooling.

The *ab* slab of $[et]_3[AuBr_4]$ **2** (Fig. 13) is comprised of two crystallographically independent et donor molecules. Four molecules of type **I** and two of type **II** make up the unit cell. While the central C–C distance in type **I** molecules [1.327(12) Å] is essentially equivalent to that observed for neutral et,[24] the elongated C–C distance in molecules of type **II** [1.370(18) Å] as well as the contracted C–S distances are indicative of a charge transfer of between 0.5 and 1.0 e.[25] The shortest intermolecular S ··· S contacts (Table 6) are observed between molecules of type **I** along zigzag chains, *A*, parallel to the crystallographic *b* axis. Intermolecular contacts *B*, between type **I** and **II** molecules, also exhibit significant S ··· S contacts. Separations within the stacks along the *a* axis are all greater than the sum of the van der Waals radii.

The lengthening of the central C–C bond in the type **II** molecules destabilises its HOMO with respect to the type **I** molecules. Our extended-Hückel calculations indicate an energy difference of 0.124 eV between the HOMOs of the two isolated molecules. Consequently, the interactions between the HOMOs of type **II** molecules are expected to determine the nature of the highest-occupied levels of the slab. However, no close contacts exist between type **II** molecules in the crystal structure of compound **2**. Since the HOMOs of the type **II** molecules can only interact through the lower-lying HOMOs of molecules of type **I** they are not expected to form dispersive bands. In contrast there is a two-dimensional network of molecules of type **I** (Fig. 13 and Table 6) where it is expected that their HOMOs will lead to dispersive bands.

Our tight-binding calculations for the *ab* slabs of et in compound **2** substantiate this analysis. The formal oxidation of the et molecules required by the stoichiometry provides ten electrons partially to fill the six HOMO bands (*i.e.* those bands derived from the HOMOs of the six et molecules in the unit cell; the screw and glide symmetry operations cause every pair of bands to be degenerate at the zone boundaries). The highest pair of these HOMO bands is very narrow and primarily derived from molecules of type **II** whereas the two lower pairs of

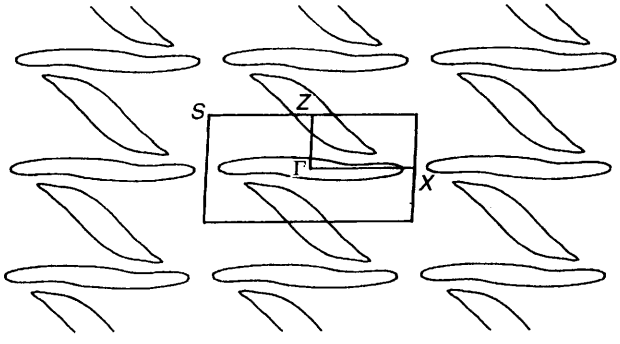

Fig. 12 Fermi surface associated with the et slab of compound **1**. The points Γ, *X*, *Z* and *S* are as defined in Fig. 11

Table 6 Intermolecular S ··· S distances less than 3.8 Å associated with the et ··· et interactions in compound **2**

Interaction	S ··· S/Å
A	3.344, 3.491, 3.582, 3.597, 3.612, 3.713, 3.720
B_1	3.470, 3.472, 3.704
B_2	3.505, 3.521, 3.526, 3.618
C_1	3.771
C_2	3.802 (× 2)

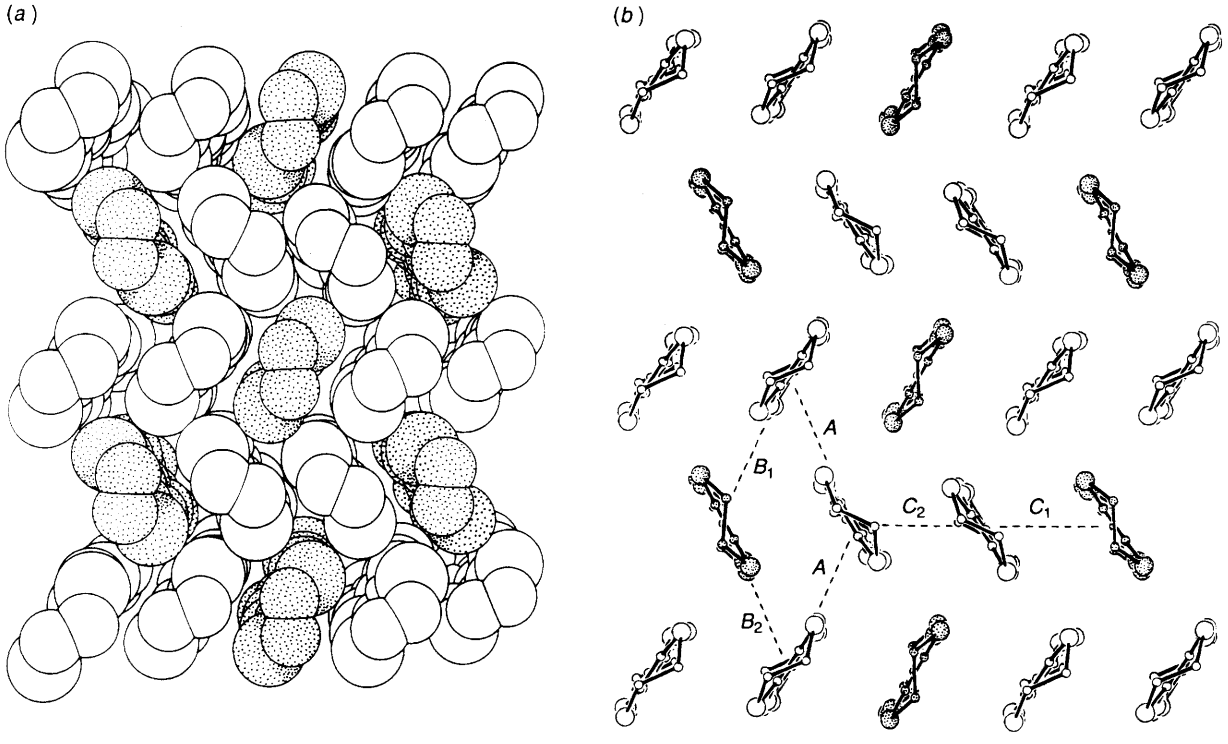

Fig. 13 Space filling (protons omitted for clarity) (*a*) and conventional ball-and-stick (*b*) views of the *ab* slab in compound **2**, looking down the et molecular plane, indicating the molecular contacts. The crystallographically independent molecules are signified using different shadings

bands are dispersive and primarily derived from molecules of type **I**. Consequently, a band description of the conducting properties of **2** is not appropriate. The two electrons per unit cell available to fill the higher-lying pair of narrow bands are most probably localised and the system should be considered as a Mott–Hubbard semiconductor.[26] In simple chemical terms, every molecule of type **I** in the lattice is et^0 and every molecule of type **II** is et^+, with one unpaired electron. Since the et^+ cations do not lie directly over each other, the anomaly in the conductivity measurements at 125 K cannot be due to a spin-Peierls transition.[27] Most likely, this transition originates from a structural change in the anion sublattice upon cooling which induces a slight change in the et slabs.

Acknowledgements

J. C. F. is grateful to the SERC and 3M for provision of a CASE award, D. J. W. to SERC for an equipment grant. The stay of James Martin at Orsay was supported by a postdoctoral fellowship from the National Science Foundation (USA) (INT-9007963). We are grateful to Professor A. E. Underhill (Bangor) for performing the conductivity measurements.

References

1 U. Geiser, B. A. Anderson, A. Murray, C. M. Pipan, C. A. Rohl, B. A. Vogt, H. H. Wang, J. M. Williams, D. B. Kang and M.-H. Whangbo, *Mol. Cryst. Liq. Cryst.*, 1990, **181**, 105.
2 H. Kobayashi, R. Kato, T. Mori, A. Kobayashi, Y. Sasaki, G. Saito and H. Inokuchi, *Chem. Lett.*, 1983, 759.
3 T. Mallah, C. Hollis, S. Bott, M. Kurmoo, P. Day, M. Allan and R. H. Friend, *J. Chem. Soc., Dalton Trans.*, 1990, 859.
4 S. S. P. Parkin, E. M. Engler, R. R. Schumaker, R. Lagier, V. Y. Lee, J. C. Scott and R. L. Greene, *Phys. Rev. Lett.*, 1983, **50**, 270.
5 J. M. Williams, M. A. Beno, H. H. Wang, P. E. Reed, L. J. Azevedo and J. E. Schirber, *Inorg. Chem.*, 1984, **23**, 1790.
6 R. P. Shibaeva, V. E. Korotkov and P. L. Rozenberg, *Sov. Phys. Crystallogr. (Engl. Transl.)*, 1991, **36**, 820; A. V. Gudenko, V. B. Ginodman, V. E. Korotkov, A. V. Koshelap, N. D. Kusch, V. N. Laukin, L. P. Rozenberg, A. G. Khomenko, R. P. Shibaeva and E. B. Yagubskii, in *The Physics and Chemistry of Organic Superconductors*, eds. G. Saito and S. Kagoshima, Springer, Berlin, 1990, p. 365; P. Day, M. Kurmoo, T. Mallah, I. R. Marsden, R. H. Friend, F. L. Pratt, W. Hayes, D. Chasseau, J. Gaultier, G. Bravic and L. Ducasse, *J. Am. Chem. Soc.*, 1992, **114**, 10722; M. Kurmoo, T. Mallah, P. Day, I. R. Marsden, M. Allan, R. H. Friend, F. L. Pratt, W. Hayes, D. Chasseau, J. Gaultier and G. Bravic, in *The Physics and Chemistry of Organic Superconductors*, eds. G. Saito and S. Kagoshima, Springer, Berlin, 1990, p. 290; T. Mallah, C. Hollis, S. Bott, P. Day and M. Kurmoo, *Synth. Met.*, 1988, **27**, A381.
7 K. S. Varma, A. Bury, N. J. Harris and A. E. Underhill, *Synthesis*, 1987, **9**, 837.
8 P. Braunstein and R. J. H. Clark, *J. Chem. Soc., Dalton Trans.*, 1973, 1845.
9 R. Uson, J. Vicente and J. Oro, *Inorg. Chim. Acta*, 1981, **52**, 29.
10 D. M. L. Goodgame, M. Goodgame and F. A. Cotton, *J. Am. Chem. Soc.*, 1961, **83**, 4160.
11 F. A. Cotton, D. M. L. Goodgame and M. Goodgame, *J. Am. Chem. Soc.*, 1961, **83**, 4690.
12 L. B. Coleman, *Rev. Sci. Instrum.*, 1975, **46**, 1125.
13 G. M. Sheldrick, SHELXTL, An integrated system, for solving refining and displaying crystal structures from diffraction data, Version 4.2, 1990, University of Göttingen.
14 M. H. Whangbo and R. Hoffman, *J. Am. Chem. Soc.*, 1978, **100**, 6093.
15 R. Hoffmann, *J. Chem. Phys.*, 1963, **39**, 1397.
16 J. H. Ammeter, H. B. Burgi, J. Thibeault and R. Hoffmann, *J. Am. Chem. Soc.*, 1978, **100**, 3686.
17 M. H. Whangbo, J. M. Williams, P. C. W. Leung, M. A. Beno, T. J. Emge, H. H. Wang, K. D. Carlson and G. W. Crabtree, *J. Am. Chem. Soc.*, 1985, **107**, 5815; E. Clementi and C. Roetti, *At. Data Nucl Data Tables*, 1974, **14**, 177.
18 J. M. Williams, H. H. Wang, T. J. Emge, U. Geiser, M. A. Beno, P. C. W. Leung, K. D. Carlson, R. J. Thorn and A. J. Schultz, *Prog. Inorg. Chem.*, 1987, **35**, 51.
19 J. C. Fitzmaurice, A. M. Z. Slawin, D. J. Williams and J. D. Woollins, *J. Chem. Soc., Chem. Commun.*, 1993, 1479.
20 A. J. Epstein, E. M. Conwell, D. J. Sandman and J. S. Miller, *Solid State Commun.*, 1981, **23**, 355; A. J. Epstein and E. M. Conwell, *Solid State Commun.*, 1977, **24**, 627.
21 M. J. Rosseinsky, M. Kurmoo, P. Day, I. R. Marsden, R. H. Friend, D. Chasseau, J. Gauttier, G. Bravic and C. Ducasse, *J. Mater. Chem.*, 1993, **3**, 801.
22 M. Kurmoo, D. Kanazawa, P. Day, I. R. Marsden, M. Allan and R. H. Friend, *Synthetic Metals*, 1993, **55**, 2347.
23 E. Canadell and M. H. Whangbo, *Chem. Rev.*, 1991, **91**, 965.
24 H. Kobayashi, A. Kobayashi, Y. Sasaki, G. Saito and H. Inokuchi, *Bull. Chem. Soc. Jpn.*, 1986, **59**, 301.
25 M. A. Beno, U. Geiser, K. L. Kostka, H. H. Wang, K. S. Webb, M. A. Firestone, K. D. Carlson, L. Nunez, M. H. Whangbo and J. M. Williams, *Inorg. Chem.*, 1987, **26**, 1912.
26 N. F. Mott, *Metal Insulator Transitions*, Barnes and Noble, New York, 1977; B. H. Brandow, *Adv. Phys.*, 1977, **26**, 651; R. J. Hoffman, *J. Chem. Phys.*, 1963, **39**, 1397.
27 J. W. Bray, L. V. Interrante, I. S. Jacobs and J. C. Bonner, in *Extended Linear Chain Compounds*, ed. J. S. Miller, Plenum, New York, 1983, vol. 3, p. 353.

Received 9*th March* 1994; *Paper* 4/01419G